

# Non-equilibrium coherence dynamics in one-dimensional Bose gases

S. Hofferberth,<sup>1,2</sup> I. Lesanovsky,<sup>3</sup> B. Fischer,<sup>2</sup> T. Schumm,<sup>1</sup> and J. Schmiedmayer<sup>1,2,\*</sup>

<sup>1</sup>Atominstytut der Österreichischen Universitäten,  
TU-Wien, Stadionallee 2, A-1020 Vienna, Austria

<sup>2</sup>Institut für Experimentalphysik, Universität Heidelberg,  
Philosophenweg 12, D-69120 Heidelberg, Germany

<sup>3</sup>Institut für Theoretische Physik, Universität Innsbruck, Technikerstr. 21a, A-6020 Innsbruck, Austria

Low-dimensional systems are beautiful examples of many-body quantum physics [1]. For one-dimensional systems [2] the Luttinger liquid approach [3] provides insight into universal properties. Much is known of the equilibrium state, both in the weakly [4, 5, 6, 7] and strongly [8, 9] interacting regime. However, it remains a challenge to probe the dynamics by which this equilibrium state is reached [10]. Here we present a direct experimental study of the coherence dynamics in both isolated and coupled degenerate 1d Bose gases. Dynamic splitting is used to create two 1d systems in a phase coherent state [11]. The time evolution of the coherence is revealed in local phase shifts of the subsequently observed interference patterns. Completely isolated 1d Bose gases are observed to exhibit a universal sub-exponential coherence decay in excellent agreement with recent predictions by Burkov et al. [12]. For two coupled 1d Bose gases the coherence factor is observed to approach a non-zero equilibrium value as predicted by a Bogoliubov approach [13]. This coupled-system decay to finite coherence is the matter wave equivalent of phase locking two lasers by injection. The non-equilibrium dynamics of superfluids plays an important role in a wide range of physical systems, such as superconductors, quantum-Hall systems, superfluid Helium, and spin systems [14, 15, 16]. Our experiments studying coherence dynamics show that 1d Bose gases are ideally suited for investigating this class of phenomena.

The starting point of our experiments is a 1d Bose gas of a few thousand atoms trapped in a highly elongated, cylindrical magnetic microtrap on an atom chip [17, 18] with typical transverse and longitudinal oscillator frequencies of  $\nu_{\perp} \sim 4.0$  kHz and  $\nu_z \sim 5$  Hz. Our trapped Bose gas is in the 1d quasi-condensate regime [1], characterized by both the temperature  $T$  and chemical potential  $\mu$  fulfilling  $k_B T, \mu < h\nu_{\perp}$  [19].

After the initial preparation of this single 1d system, we perform a phase-coherent splitting along the transverse direction by means of a radio-frequency (rf) induced adiabatic potential [11]. As shown in figure 1, the final system consists of two 1d quasi-condensates in a vertically orientated double-well potential [20]. They are sep-

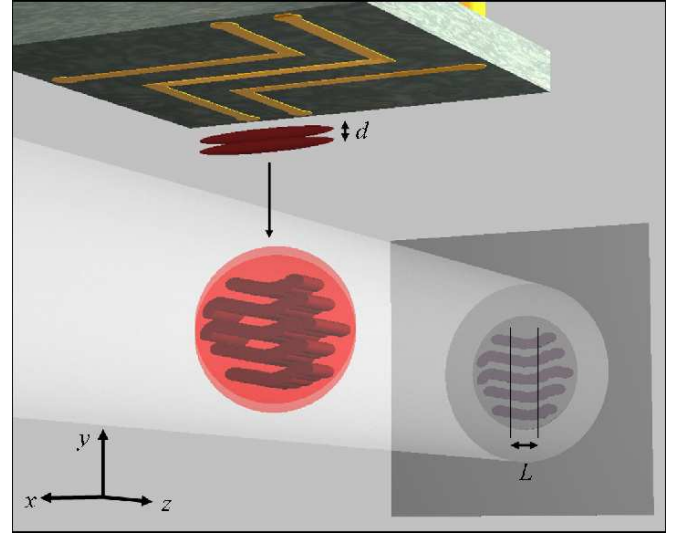


FIG. 1: Schematic of the experiment. A single 1d quasi-condensate is phase coherently split using rf potentials on an atom chip. A combination of two rf fields allows balanced splitting in the vertical direction [20]. After the separation, the system is held in the double-well potential for a variable time  $t$  and is then released from the trap. The resulting interference pattern is imaged along the transverse direction of the system. Thermal phase fluctuations in the two quasi-condensates can be directly observed as local shifts of the observed fringe profiles.

arated by a tunable potential barrier, whose height is controlled by the applied rf fields.

This splitting process initializes the system in a mutually phase coherent state. Directly after the splitting, the phase fluctuation patterns of the two individual quasi-condensates are identical, resulting in a vanishing global relative phase. This is a highly non-equilibrium state of the split system, which will relax to equilibrium over time.

To study this time evolution of the phase coherence, the two 1d Bose gases are held in the double-well configuration for a varying time  $t$  before they are released and recombined in time-of-flight. The resulting interference pattern is recorded using standard absorption imaging along the transverse direction of the system. The spatial variation of the relative phase between the two quasi-condensates translates directly into local phase shifts in the interference pattern (Figure 2).

If the two parts of the system are completely separated (compare methods), the equilibrium state consists of two uncorrelated quasi-condensates. Consequently, we observe an increasing waviness of the interference pattern with time, which in the end leads to a complete randomization of the relative phase  $\theta(z, t)$  (Figure 2a, b). This change in the interference pattern is a direct visualization of the dynamics of the phase fluctuations. Qualitatively similar behavior was recently observed at MIT [21] for elongated condensates with  $\mu \sim 2h\nu_{\perp}$  and  $T \sim 5h\nu_{\perp}$ .

For a finite tunnel coupling (compare methods) between the two systems, we also observe an increase in the waviness of the interference. However, in contrast to the completely separated case, the final equilibrium state shows a non-random phase distribution (Figure 2c,d). This is caused by the phase randomization being counterbalanced by the coherent particle exchange between the two fractions. The final width of the observed phase spread depends on the strength of the tunnel coupling [22, 23].

A quantitative measure of the fluctuations of the local relative phase is given by the coherence factor

$$\Psi(t) = \frac{1}{L} \left| \int dz e^{i\theta(z,t)} \right| \quad (1)$$

where  $L$  is the length of the analyzed signal.

We obtain the coherence factor from a single image by extracting the local relative phase  $\theta(z, t)$  from the interference pattern in each vertical pixel slice. To account for variations in the 1d atomic density  $n_{1d}(z)$  due to the longitudinal confining potential, we use only the central 40% of each image in our analysis. Over this range,  $n_{1d}(z)$  varies by only  $\sim 15\%$  from its peak value. In the following, we neglect this modulation and assume a homogeneous density, obtained by averaging over the density profile in this center region.

We first investigate the time evolution of the coherence factor  $\Psi(t)$  for the case of completely separated 1d quasi-condensates, separated by a potential barrier sufficiently high to suppress any tunnel coupling (Figure 2a,b). The time evolution of the measured coherence factor for six different combinations of initial temperature  $T_{\text{in}}$ , 1d density  $n_{1d}$ , and transverse trap frequency  $\nu_{\perp}$  is displayed in figure 3. In a time window of 1-12 ms we observe a universal sub-exponential decay of the form

$$\Psi(t) \propto e^{-(t/t_0)^{\alpha}}, \quad (2)$$

with decay time constants  $t_0$  ranging from 5 ms to 9 ms (Table I).

Our results can be directly compared with a recent theoretical study by Burkov *et al.* [12] based on a Luttinger liquid approach [3], which predicts  $\alpha = 2/3$  for the exponent in Eq. 2. For all the cases studied, we find  $\alpha$  to be between 0.64 and 0.67 (Table I), in very good agreement with the theoretical prediction. This agreement is even

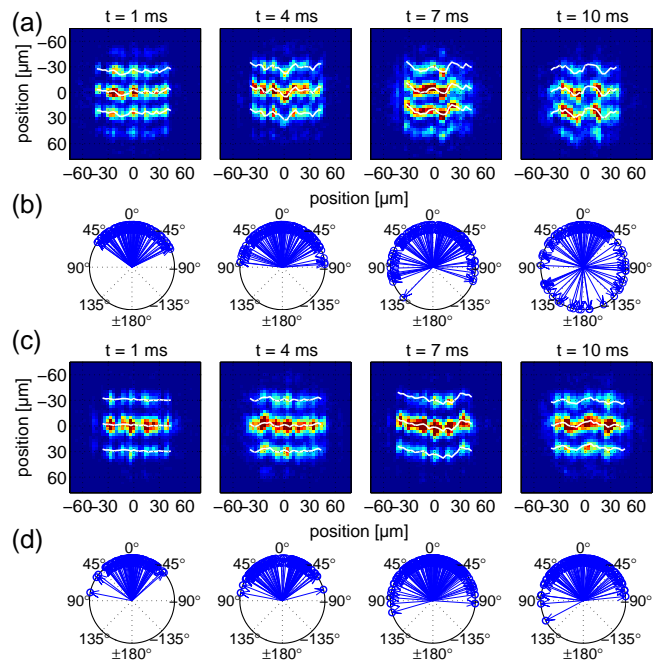


FIG. 2: Direct observation of the phase dynamics through interference. (a) Example images of the observed interference patterns for hold times  $t = 1, 4, 7, 10$  ms in the case of isolated 1d systems (taken from the  $T = 133$  nK data set in figure 3b). White lines indicate the bright nodes of the local interference pattern, extracted from fits to the profiles in each vertical pixel slice. The randomization of the relative phase  $\theta(z, t)$  over time leads to an increased waviness of the observed fringe patterns. (b) Corresponding polar plots of the local relative phases from the central regions of five images. For the isolated systems we find a complete randomization of the local relative phase over time. (c) For a finite tunnel coupling through the potential barrier, the phase randomization is counterbalanced by particle tunnelling, resulting in a suppression of the fringe waviness (images correspond to figure 4(c)). (d) This results in a non-random steady-state phase spread, whose width depends on the tunnel coupling and the temperature of the system.

$T_{\text{in}}$ [nK]	$n_{1d}$ [1/μm]	$\mu/h$ [kHz]	$\nu_{\perp}$ [kHz]	$\alpha$	$t_0$ [ms]	$T_f$ [nK]
82(28)	20(4)	0.7(1)	3.3	0.64(8)	9.0(4)	76(10)
133(25)	34(5)	1.2(2)	3.3	0.65(7)	5.5(3)	145(13)
171(19)	52(4)	1.8(1)	3.3	0.64(4)	6.4(3)	186(15)
81(31)	22(4)	0.9(2)	4.0	0.65(3)	8.1(2)	85(10)
128(23)	37(4)	1.5(2)	4.0	0.66(3)	5.9(2)	153(13)
175(20)	51(5)	2.1(2)	4.0	0.64(6)	6.1(4)	194(17)

TABLE I: Measured exponents  $\alpha$ , decay time constants  $t_0$  and final temperatures  $T_f$  after the splitting for the data shown in figure 3.

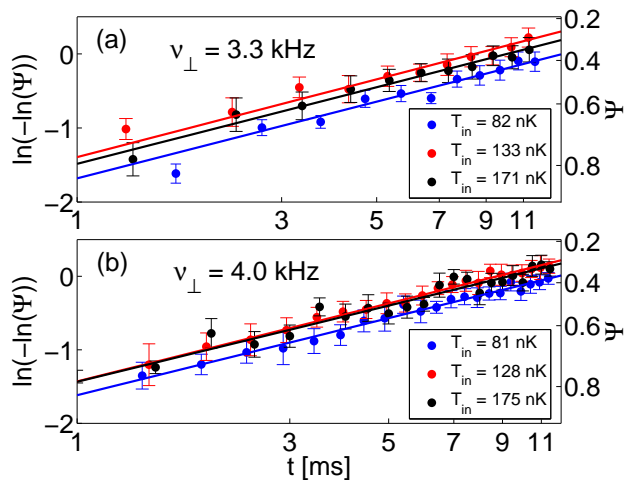


FIG. 3: Time evolution of the coherence factor for uncoupled 1d quasi-condensates. Double logarithmic plots of  $\ln(\Psi)$  as a function of time  $t$  for transverse confinements of (a)  $\nu_{\perp} = 3.3$  kHz and (b)  $\nu_{\perp} = 4.0$  kHz, respectively. Three different data sets corresponding to different initial temperatures and line densities are shown for each configuration. Each data point is the average of 15 individual measurements. Error bars indicate the standard error of the mean. In this representation, the exponent of the decay function is given directly by the slope of the observed linear evolution of  $\ln(\Psi)$ . The lines shown are linear fits to the data, the obtained slopes are  $0.64 \pm 0.08$ ,  $0.65 \pm 0.07$ , and  $0.64 \pm 0.04$  for (a) and  $0.65 \pm 0.03$ ,  $0.66 \pm 0.03$ , and  $0.64 \pm 0.06$  for (b). All slopes show good agreement with the theoretical prediction of  $2/3$ .

more remarkable because the approximations used in ref. [12] to obtain Eq. 2 and  $\alpha = 2/3$  are only valid for  $t > t_0$ , whereas our data covers the full range from 0 up to  $2 t_0$ .

At our typical temperatures ( $T_{\text{in}} \approx 80 - 150$  nK), the dynamics of the coherence factor is dominated by thermal phase fluctuations [12, 24]. Burkov *et al.* derive the decay of  $\Psi(t)$  by assuming that the system of two 1d Bose gases can evolve into thermal equilibrium. The sub-exponential coherence decay then results from the fact that damping in a 1d liquid at finite temperature is always non-hydrodynamic, which in turn is caused by the break-down of superfluid order in 1d on length scales longer than the temperature-dependent correlation length [25]. The experimentally observed decay agrees with this non-trivial theoretical prediction, which is strong evidence that the final equilibrium state of our system is truly thermal equilibrium. In turn, this suggests the non-integrability of the experimentally realized system [26].

Following ref. [12] the decay time constant  $t_0$  can be related to the parameters of the 1d quantum gas:

$$t_0 = 2.61 \pi g n_{1d} K / T_f^2 \quad (3)$$

where  $K = \pi \hbar \sqrt{\frac{n_{1d}}{gm}}$  is the Luttinger parameter for the weakly interacting 1d Bose gas [27].  $g = 2\hbar v_{\perp} a_s$  is the

effective 1d coupling constant with  $a_s$  being the s-wave scattering length,  $m$  the mass of the atoms, and  $T_f$  the final equilibrium temperature of the split system.

$T_f$  can be extracted from the decay constant  $t_0$  following Eq. 3 using independently measured values of  $\nu_{\perp}$  and  $n_{1d}$ . The results, together with an independently measured initial temperature of the unsplit system  $T_{\text{in}}$  from time-of-flight images, are compiled in table I. Within the error bounds, the temperatures  $T_{\text{in}}$  and  $T_f$  agree. Never the less, our data seems to indicate an increasing difference between  $T_{\text{in}}$  and  $T_f$  for increasing initial temperature.

This observation is in qualitative agreement with ref [12], which predicts the heating during the splitting to scale with  $\sqrt{T_{\text{in}} K}$ . This is also supported by the observation that for identical  $T_{\text{in}}$ , we find the same temperature increase in the split system for both of the two different transverse confinements used in the experiment.

One should note here that the temperature  $T_f$  is the temperature of the longitudinal excitations and is measured on a time scale much shorter than the characteristic time given by the sound propagation through the sample, or a thermalization timescale, which should be even longer. To check the universality of our experiments, we cut each sample in two and analyze each half separately. We obtain the same results within the statistical uncertainties.

We now turn to the case of (weakly) coupled 1d quasi-condensates realized when the potential barrier between the two 1d systems is only slightly larger than the chemical potential  $\mu$ , and tunnelling between the two split systems is significant. In this case we observe a qualitative change in the behavior of the coherence factor  $\Psi(t)$ , as illustrated in figure 4. After an initial decay, the coherence factor saturates well above the value for random phases. This observation is a clear manifestation of a balancing between phase locking due to coherent tunnelling and the local phase fluctuations in the 1d quasi-condensate [13]. It is the matter wave equivalent of injection locking two lasers.

For a quantitative analysis, we use the results of ref. [13] for the energy spectrum and the mode functions and express the final equilibrium coherence factor as

$$\Psi = \Psi_q \times \exp \left( -\frac{1}{4\pi n_{1d}} \int dk \frac{S_k}{e^{\frac{\epsilon_k}{k_B T}} - 1} \right), \quad (4)$$

where  $\Psi_q (\approx 1$  in our case) is the contribution of the quantum fluctuations, and

$$\begin{aligned} \epsilon_k &= \sqrt{\left( \frac{\hbar^2 k^2}{2m} + 2\gamma \right) \left( \frac{\hbar^2 k^2}{2m} + 2\gamma + 2gn_{1d} \right)} \\ S_k &= \sqrt{\frac{\frac{\hbar^2 k^2}{2m} + 2\gamma + 2gn_{1d}}{\frac{\hbar^2 k^2}{2m} + 2\gamma}} \end{aligned} \quad (5)$$

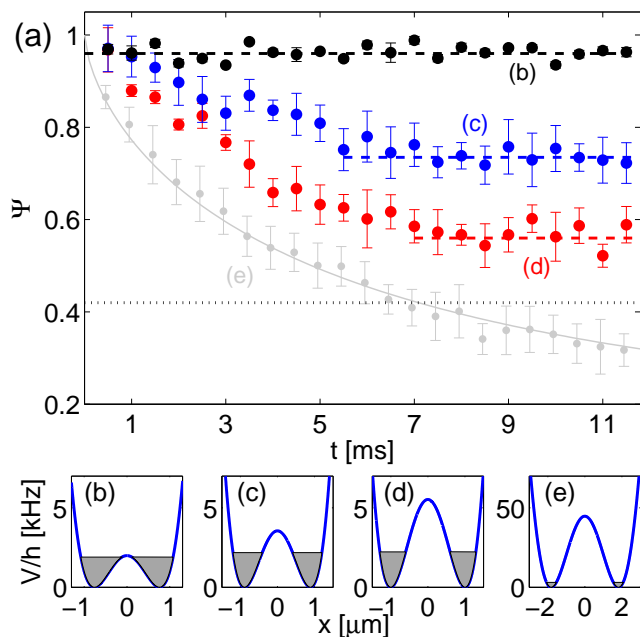


FIG. 4: Time evolution of the coherence factor for coupled 1d quasi-condensates. (a) After an initial decay we observe a time-independent coherence factor determined by the strength of the tunnel coupling. Different colors correspond to the different transverse double-well potentials shown in (b-d) as indicated. Each data point is the average of 12 individual measurements. Error bars indicate s.e.m. The light grey points are the  $T = 128$  nK data set from figure 3b, showing the sub-exponential decay in the case of uncoupled condensates for comparison. The corresponding transverse potential is shown in (e). The dotted black line in (a) indicates the Rayleigh test confidence level above which the considered phase distribution of a single measurement can be identified as non-random with a 90% probability. In the coupled case, the final phase distribution in each realization can be clearly considered as non-random.

are the energy eigenvalues and amplitudes of the Bogoliubov modes, respectively.  $\gamma$  thereby quantifies the tunnel coupling between the two 1d systems. Independent measurements of  $T$  and  $n_{1d}$  allow us to extract  $\gamma$  directly from the measured equilibrium coherence factors. For the red, blue, and black data sets in figure 4, we obtain  $\frac{\gamma}{gn_{1d}} \approx 0.003, 0.01, \text{ and } 0.2$ , respectively. Comparison with numerical calculations of the tunnel coupling, based on the spatial overlap of the wave functions [28], yields qualitative agreement within a factor of three. This suggests that a two-mode model for the tunnelling dynamics is not sufficient to describe our experiments. Alternatively, if  $\gamma$  can be determined independently, the equilibrium coherence factor can be used for thermometry in the coupled system [23].

Particle exchange between the two condensates takes place on a timescale given by the inverse of the Josephson

oscillation frequency [13]

$$\omega_J = \frac{\sqrt{\gamma gn_{1d}}}{\hbar}. \quad (6)$$

From our measured  $\gamma$  we estimate  $\omega_J \approx 2\pi \times 80, 200, 900$  Hz for the three presented data sets, which should be compared to the coherence decay time scale of the order of 5 ms (Figure 4). This suggests that the balancing process between coherent tunnelling and phase fluctuations stabilizes on timescales of the order of a single or few Josephson oscillations in a coupled 1d system.

In summary, we have studied the non-equilibrium phase dynamics in a 1d Bose gas with the aid of matter wave interferometry. For completely separated systems we observe the sub-exponential coherence decay predicted by Luttinger liquid theory [12]. For coupled 1d Bose gases, the balance between decoherence and phase stabilization due to tunnelling establishes a finite coherence [13, 23]. In both examples our experiments illustrate how the thermal equilibrium state of a phase-fluctuating 1d quasi-condensate [1, 4, 5, 6, 7] is approached from the highly non-equilibrium situation of two phase coherent copies created by splitting a degenerate 1d Bose gas.

The above investigation demonstrates that with the exquisite control provided by atom chips, one can now study in detail the non-equilibrium dynamics of coherence in a single quantum degenerate 1d system. This allows us to address the fundamental issue of thermalization in (almost) integrable systems [26]. Our approach can easily be extended to study the dynamics of two- and three-dimensional quantum systems, and to include other factors such as internal state dynamics. Moreover, it will be the starting point for detailed studies of coupled 1d quantum systems. One prominent example is the quantum Sine-Gordon model, which plays an important role in many fundamental physics questions [2, 29, 30, 31].

### Acknowledgement

We thank A. Burkov, V. Gritsev, E. Demler, R. Bistritzer, and E. Altman for stimulating discussions. We also thank S. Groth for fabricating the atom chip used in the experiments. We acknowledge financial support from the Wittgenstein Prize and the European Union, through Atom Chips and FET/QIPC SCALA projects.

### Methods

#### Preparing a 1d BEC on an atom chip

We start by preparing a magnetically trapped ultra cold ( $T \sim 1\mu\text{K}$ ) sample of  $\text{Rb}^{87}$  atoms in the  $|F = 2, m_F = 2\rangle$  state on the atom chip [17, 18] using our standard procedure of laser cooling, magnetic trapping

and evaporative cooling [32]. The sample is then transferred to a highly elongated magnetic trap ( $\nu_{\perp} \sim 4.0$  kHz, longitudinal confinement  $\nu_z < 5$  Hz) at a distance of  $75 \mu\text{m}$  from the atom chip surface and cooled to quantum degeneracy by tuning the evaporative cooling radio frequency (rf) in between the ground and first excited transverse trapping state. The resulting sample an effectively one-dimensional [4, 19] with  $\mu, k_{\text{B}}T < h\nu_{\perp}$  containing  $1 \dots 10 \times 10^3$  atoms.

### Smoothness of the trapping potentials

Our atom chip wires [33] provide exceptionally smooth trapping potentials [34]. The residual roughness due to current-flow perturbations in the trapping wire is much too small to be measured directly at our operation distance  $h = 75 \mu\text{m}$  from the atom chip surface. An estimate based on the current flow pattern in the wire reconstructed from magnetic field microscopy measurements employing 1d condensates at short distance ( $\sim 10 \mu\text{m}$ ) [35] shows that for length scales below  $40 \mu\text{m}$ , the remaining potential perturbations are smaller than  $1 \mu\text{G}$  (corresponding to  $< 10^{-3} \mu$ ). Due to the exponential damping of the higher spatial modes (wave vector  $k = \frac{2\pi}{\lambda}$ ) of the magnetic field variations with distance  $h$  from the chip surface following  $\exp(-kh)$ , the disorder potentials will be even smaller on the short length scales corresponding to the phase coherence length or the healing length in the 1d Bose gas.

### Preparing two phase-coherent 1d systems

To prepare two mutually phase coherent 1d systems, we employ a combination of static and rf magnetic fields on our atom chip. Coupling electronic ground states of the magnetically trapped atoms results in dressed-state adiabatic potentials, whose versatility stems from the dependence of the potential on the angular orientation between the rf field and the static trapping field [36]. In particular, one can create very robust double-well potentials, which allow the coherent splitting of a trapped Bose condensate [11]. In the experiments presented here, we employ a setup similar to that in ref. [20] where the combination of two rf fields generated by auxiliary wires on the atom chip allows the realization of a compensated double-well potential in the vertical plane. For this double-well orientation, the observed interference fringes in the atomic density are horizontal, parallel to the atom chip surface. This allows us to image the interference pattern along the transverse direction of the system (Figure 1).

### Preparing two 1d systems with a variable tunnel coupling

To introduce a variable tunnel coupling between the two 1d systems, we adjust the potential barrier between 3 and 8 kHz by changing the amplitude of the rf fields (Figure 4). The actual barrier height is determined from spectroscopic measurements of the rf potentials to a precision  $< 1$  kHz [37]. To evaluate whether the two samples in the resulting double-well potential can be considered as one-dimensional, we compare the chemical potential  $\mu$  and the thermal energy  $k_{\text{B}}T$  of the trapped ensembles to the single-particle level spacing in the double-well. In the case of large potential barriers, the transverse confinement of each individual well can be approximated by a harmonic oscillator, and the level spacing is given by the oscillator frequency  $\nu_{\perp}$ . For small barriers, this approximation fails and one has to numerically calculate the single particle states in the transverse double-well potential. For the configurations shown in figure 4 (b-d), we find energy separations between the ground-state doublet and first excited states of  $\Delta = 2.8, 3.4, 3.8$  kHz, respectively. Consequently,  $\mu, k_{\text{B}}T \leq h\Delta$  for all configurations, justifying the 1d treatment of the individual systems.

### Measuring the interference pattern and extracting the local relative phase

We observe the interference pattern created by the two expanding, overlapping atomic clouds using standard absorption imaging. Employing diffraction-limited optics, optimized light path and pulse duration, and a weak magnetic field to define a quantization axis, we achieve atom shot noise limited imaging with  $3 \mu\text{m}$  resolution and a noise floor of  $\sim 3$  atoms per  $3 \times 3 \mu\text{m}$  pixel. We extract the local relative phase  $\theta(z)$  by fitting a cosine function with a Gaussian envelope to the observed density distribution in each individual vertical pixel slice. The free parameters of these fits are the relative phase  $\theta$ , the contrast, and the fringe spacing. The width, amplitude, and center position of the envelope are determined independently from a Gaussian fit to the total integrated density pattern of the central area of each image. From the measured phases, the coherence factor is evaluated (compare eq. 1). This has to be contrasted to the methods used in ref. [23, 38], where the interference patterns are summed up and the contrast is analyzed.

### Evaluating the coherence decay constant

Several aspects must be considered when evaluating the decoherence constant  $t_0$ . First, the time  $t = 0$  when the tunnel coupling vanishes and the two condensates start to evolve independently, changes for different



atomic densities and trap parameters and has to be evaluated for each data set separately. Higher atomic densities [39], or stronger transverse confinement lead to increased tunnel coupling as the overlap of the two matter waves in the tunnelling region becomes larger [40]. The moment of the decoupling of the two systems can be estimated by numerically calculating the time-dependent tunnel coupling throughout the splitting. Experimentally, one observes a qualitative change in the detected interference patterns [11, 20, 41] when the barrier becomes higher than the chemical potential. In the case of the widely split independent condensates, the uncertainty in the determination of  $t = 0$  is much smaller than 1 ms.

The second aspect to consider is that for a finite system length  $L$ , the coherence factor does not approach zero but converges to a finite value. The average coherence factor calculated from a limited number of samples is non-zero, even if these phases are totally random. Such a limited number of samples for a system of length  $L$  is given by the finite imaging resolution, and by the finite phase-coherence length itself [4], which in our case is comparable to a single pixel width. This results in an additional offset in the equilibrium coherence factor, which can be determined from the number of data points used in the calculation of  $\Psi$  [42].

---

\* Electronic address: schmiedmayer@atomchip.org

- [1] Popov, V. N. *Functional Integrals in Quantum Field Theory and Statistical Physics* (Reidel, Dordrecht, 1983).
- [2] Giamarchi, T. *Quantum Physics in One Dimension* (Oxford University Press, 2003).
- [3] Haldane, F. Effective harmonic-fluid approach to low-energy properties of one-dimensional quantum fluids. *Phys. Rev. Lett.* **47**, 1840–1843 (1981).
- [4] Petrov, D. S., Shlyapnikov, G. V. & Walraven, J. T. M. Regimes of quantum degeneracy in trapped 1D gases. *Phys. Rev. Lett.* **85**, 3745–3749 (2000).
- [5] Dettmer, S. *et al.* Observation of phase fluctuations in elongated Bose-Einstein condensates. *Phys. Rev. Lett.* **87**, 160406 (2001).
- [6] Richard, S. *et al.* Momentum spectroscopy of 1D phase fluctuations in Bose-Einstein condensates. *Phys. Rev. Lett.* **91**, 010405 (2003).
- [7] Pricoupenko, L., Perrin, H. & M. Olshanii, e. *Quantum gases in low dimensions*, vol. 116 (2004). For an overview see.
- [8] Paredes, B. *et al.* Tonks-Girardeau gas of ultracold atoms in an optical lattice. *Nature* **429**, 277–281 (2004).
- [9] Kinoshita, T., Wenger, T. & Weiss, D. S. Observation of a one-dimensional Tonks-Girardeau gas. *Science* **305**, 1125–1128 (2004).
- [10] Kinoshita, T., Wenger, T. R. & Weiss, D. S. A quantum Newton’s cradle. *Nature* **440**, 900–903 (2006).
- [11] Schumm, T. *et al.* Matter wave interferometry in a double well on an atom chip. *Nature Phys.* **1**, 57–62 (2005).
- [12] Burkov, A. A., Lukin, M. D. & Demler, E. Decoherence dynamics in low-dimensional cold atoms interferometers. *Phys. Rev. Lett.* **98**, 200404 (2007).
- [13] Whitlock, N. K. & Bouchoule, I. Relative phase fluctuations of two coupled one-dimensional condensates. *Phys. Rev. A* **68**, 053609 (2003).
- [14] Blatter, G., Feigelman, M., Geshkenbein, V., Larkin, A. & Vinokur, V. Vortices in high-temperature superconductors. *Rev. Mod. Phys.* **66**, 1125 (1994).
- [15] Shimshoni, E., Auerbach, A. & Kapitulinik, A. Transport through quantum melts. *Phys. Rev. Lett.* **80**, 3352–3355 (1998).
- [16] Forte, S. Quantum mechanics and field theory with fractional spin and statistics. *Rev. Mod. Phys.* **64** (1992).
- [17] Folman, R., Krüger, P., Schmiedmayer, J., Denschlag, J. & Henkel, C. Microscopic atom optics: from wires to an atom chip. *Adv. At. Mol. Opt. Phys.* **48**, 263–356 (2002).
- [18] Fortagh, J. & Zimmermann, C. Magnetic microtraps for ultracold atoms. *Rev. Mod. Phys.* **79**, 235 (2007).
- [19] Bouchoule, I., Kheruntsyan, K. V. & Shlyapnikov, G. V. Interaction-induced crossover versus finite-size condensation in a weakly interacting trapped one-dimensional Bose gas. *Phys. Rev. A* **75**, 031606(R) (2007).
- [20] Hofferberth, S., Lesanovsky, I., Fischer, B., Verdu, J. & Schmiedmayer, J. Radio-frequency dressed state potentials for neutral atoms. *Nature Phys.* **2**, 710–716 (2006).
- [21] Jo, G. B. *et al.* Matter-wave interferometry with phase fluctuating bose-einstein condensates (2007). ArXiv:0706.4041.
- [22] Spietz, L., Lehnert, K. W., Siddiqi, I. & Schoelkopf, R. J. Primary electronic thermometry using the shot noise of a tunnel junction. *Science* **300**, 1929–1932 (2003).
- [23] Gati, R., Hemmerling, B., Fölling, J., Albiez, M. & Oberthaler, M. K. Noise thermometry with two weakly coupled Bose-Einstein condensates. *Phys. Rev. Lett.* **96**, 130404 (2006).
- [24] Bistrizter, R. & Altman, E. Intrinsic dephasing in one dimensional ultracold atom interferometers. *Proc. Natl. Acad. Sci. USA* **104**, 9955–9959 (2007).
- [25] Andreev, A. F. The hydrodynamics of two-dimensional and one-dimensional fluids. *Sov. Phys. JETP* **51**, 1038–1040 (1980).
- [26] Rigol, M., Dunjko, V., Yurovsky, V. & Olshanii, M. Relaxation in a completely integrable many-body quantum system: An ab initio study of the dynamics of the highly excited states of 1d lattice hard-core bosons. *Phys. Rev. Lett.* **98**, 050405 (2007).
- [27] Cazalilla, M. Bosonizing one-dimensional cold atomic gases. *J. Phys. B.: At. Mol. Opt. Phys.* **37**, S1–S47 (2004).
- [28] Ananikian, D. & Bergeman, T. The Gross-Pitaevskii equation for Bose particles in a double well potential: Two mode models and beyond. *Phys. Rev. A* **73**, 013604 (2006).
- [29] Bouchoule, I. Modulational instabilities in Josephson oscillations of elongated coupled condensates. *Eur. Phys. J. D* **35**, 147–154 (2005).
- [30] Gritsev, V., Polkovnikov, A. & Demler, E. Linear response theory for a pair of coupled one-dimensional condensates of interacting atoms. *Phys. Rev. B* **75**, 174511 (2007).
- [31] Gritsev, V., Demler, E., Lukin, M. & Polkovnikov, A. Analysis of quench dynamics of coupled one dimensional condensates using quantum sine Gordon model. ArXiv:cond-mat/0702343.
- [32] Wildermuth, S. *et al.* Optimized magneto-optical trap

- for experiments with ultracold atoms near surfaces. *Phys. Rev. A* **69**, 030901 (2004).
- [33] Groth, S. *et al.* Atom chips: Fabrication and thermal properties. *Appl. Phys. Lett.* **85**, 2980–2982 (2004).
- [34] Krüger, P. *et al.* Disorder potentials near lithographically fabricated atom chips. *eprint arXiv:cond-mat/0504686* (2004).
- [35] Wildermuth, S. *et al.* Sensing electric and magnetic fields with Bose-Einstein condensates. *Appl. Phys. Lett.* **88**, 264103 (2006).
- [36] Lesanovsky, I. *et al.* Adiabatic radio frequency potentials for the coherent manipulation of matter waves. *Phys. Rev. A* **73**, 033619 (2006).
- [37] Hofferberth, S., Fischer, B., Schumm, T., Schmiedmayer, J. & Lesanovsky, I. Ultracold atoms in radio-frequency dressed potentials beyond the rotating-wave approximation. *Phys. Rev. A* **76**, 013401 (2007).
- [38] Hadzibabic, Z., Krüger, P., Cheneau, M., Battelier, B. & Dalibard, J. Berezinskii-Kosterlitz-Thouless crossover in a trapped atomic gas. *Nature* **441**, 1118 (2006).
- [39] Gerbier, F. Quasi-1d Bose-Einstein condensates in the dimensional crossover regime. *Europhys. Lett.* **66**, 771 (2004).
- [40] Smerzi, A., Fantoni, S., Giovanazzi, S. & Shenoy, S. R. Quantum coherent atomic tunneling between two trapped Bose-Einstein condensates. *Phys. Rev. Lett.* **79**, 4950–4953 (1997).
- [41] Röhrl, A., Naraschewski, M., Schenzle, A. & Wallis, H. Transition from phase locking to the interference of independent Bose condensates: Theory versus experiment. *Phys. Rev. Lett.* **78**, 4143–4146 (1997).
- [42] Fisher, N. I. *Statistical analysis of circular data* (Cambridge University Press, 1993).